SUPPLEMENTAL DATA

Figure S1. Analysis of wild-type cells, Related to Figure 1
(A) 3D distribution of Ndc80p (green) and Spc42p (red) for a cell in mitosis. Planes for intensity projections are indicated by gray particles.
(B) Distribution of the relative intensity difference between Ndc80 for cells with spindle lengths 1.0–1.3 μm (bottom), 1.3–1.7 μm (middle), and 1.7–2 μm (top).
(C) Model of a bilobed distribution of kinetochores mediated by complete bipolarity
(D) Model of a bilobed distribution of kinetochores mediated by tensionless bipolar attachments (unseparated sisters).
(E) Model of a bilobed distribution of kinetochores mediated by a mixture of bipolar attachments under tension, tensionless bipolar attachments, and syntelic attachments.
(F) Four representative time-points of a movie with one hyper-stretched CEN IV-tag. The arrow heads indicates where the centromere proximal tag recoils after t = 111 s.

Figure S2. Classification of spindles in CEN IV assays, Related to Figure 1
(A) Scatter plot of spindle length vs. ratio of mean CEN IV-tag intensity to mean SPB-tag intensity for all time points in 47 movies of WT cells filmed in the CEN IV-tracking assay. Red dots, time points with separated CEN IV tags; blue dots, time points with unseparated tags. Separated tags display a lower intensity ratio.
(B) Probability distributions of mean CEN IV-tag intensity to mean SPB-tag intensity. Blue and red colors as in (A). Lines represent $P(i \mid s)$, the probability of a given intensity for a tag in a state s = separated or s = unseparated. Best fits are obtained using a gamma distribution
(C, D) Raw (C) and normalized (D) distributions of time points with unseparated (blue), separated (red) tags obtained from 47 movies as a function of spindle length. Black line in (D) defines $P(s \mid l)$, i.e. the probability for detecting state s at a given spindle length l.
(E) Brightfield image of wild-type cells overlaid by XY-positions of fluorescent tags detected in 3D. Different colors indicate tag association with individual spindles
(F) Tag association to spindles by hierarchical clustering
(G) Maximum intensity projection of the fluorescence images and clustered tag positions for cells in G1 (turquoise) and in mitosis (yellow and green)
(H) Zoom into the clustering tree with leaves corresponding to the tags illustrated in (G).

Figure S3. Analysis of cells with symmetric CEN IV tag design, Related to Figure 1
(A) Schematic of original asymmetric (top) and new symmetric (bottom) tag design. (2) denotes the centroid of the Tet operators in the asymmetric tag design. Assuming a chromatin density of 125 bp/nm (Bystricky et al., 2004), centroid (2) is ~50 nm away from the actual position of the centromere. In the new symmetric tag design, centroids of each 6kb Tet operators are located in (3), and the overall centroid is located on top of the centromere, denoted by (1). Note that all centroids are within the Airy disk (green disk) centered on the centromere.
(B) Schematic of two scenarios in which parts of the symmetric TetO/TetR-GFP arrays unravel. Top, for a short spindle (~1.2 μm) with bipolar attachment the full intensity of the sister tags may be located within the Airy disk centered on the centromere. This fusion spot can be erroneously classified as unseparated. However, the probability of

these misclassification decreases rapidly with longer spindles, in which the inter-kinetochore distance grows proportionately with the increasing SPB–SPB distance. Bottom, for a long spindle, when both tags are stretched, only ~40% of the intensity is located within the Airy disk centered on the centromere, i.e. the resulting spot image does no longer have the properties of a diffraction-limited signal. This situation is robustly detected either by statistically testing the residuals of PSF-mixture fits to the spot ('CEN IV-tag tracking with super-resolution'), or in case of hyper-stretching by the intensity-based reclassification ('Reclassification of unseparated tags in CEN IV-snapshot assay'), which both result in a classification of the deformed spot signal as originating from bipolar attachment.
(C) Scatter plot of spindle length vs. ratio of mean CEN IV-tag intensity to mean SPB-tag intensity for all time points in 94 movies of WT cells filmed in the CEN IV-tracking assay.
(D) Probability distributions of mean CEN IV-tag intensity to mean SPB-tag intensity. Blue and red colors as in (B). See Figure S2B for definition of fit lines.
(E, F) Raw (E) and normalized (F) distributions of time points with unseparated (blue), separated (red) tags obtained from 94 movies as a function of spindle length. See Figure S2D for definition of fit line in (F).
(G, H) Plots as in Figures 1J and 1L analyzing n = 925 mitotic cells with the symmetric CEN IV tag in the CEN IV-snapshot assay.
(I) Classification of WT spindles with unseparated (blue), separated (light red), and reclassified as separated (dark red) CEN IV-tags. Data from Figure 1L remapped as a function of time since spindle pole separation. Black dots and error bars (Mean ± SD of 1000 bootstrap samples), experimental data points for percentage of chromosomes with syntelic attachments.
(J) Red dots are the predicted FRAP recovery based on our observed percentage of syntelic attachments in (I). Bars indicate standard deviation predicted from 1000 bootstrap samples as in (H). Solid line represents our estimated total recovery at anaphase. Dashed lines represent standard deviations.

Figure S4. Tubulin signal for wild-type and mutant cells, Related to Figure 3
(A–C) Symmetrized tubulin distribution for: (A) wild-type cells, (B) *stu2-277* cells and (C) *cin8Δ* cells. For comparison of the distributions the Tub1-GFP signal is normalized to a range [0,1] for each condition.

Figure S5. Characteristic time for the resolution of one syntelic attachment in WT and *ipl1-321* cells. Related to Figure 5
(A, B) Dots represent the percentage of syntelic attachments as a function of time (see Supplemental Experimental Methods) for WT (A) and *ipl1-321* (B) cells. Lines are best fits of an exponential decay function reflecting resolution of syntely as a purely random process with characteristic time as fit parameter.

Movie S1. Gallery of images of wild-type cells in kinetochore-snapshot assay. Related to Figure 1
Images show intensity projections on plane containing SPB-SPB axis of Spc42-CFP (red) and Ndc80-GFP (green). Note the nearly constant distance between Ndc80 bilobes and their proximal SPB as the spindle length increases. Numbers indicate spindle length in microns.

Movie S2. Two examples of wild-type cells (back to back) with separated tags in CEN IV-tracking assay. Related to Figure 1
XY- (upper left), YZ- (upper right), and XZ- (lower left) intensity projections of CEN IV and SPB tags overlaid by computer-tracked locations (circles). Asterisks indicate interpolated positions of untracked tags. Time shown in minutes. Anaphase onset in the second cell is marked by rapid divergence of SPB tags after 1:00. Note that after anaphase onset the automated tracking mostly fails because the spots are close to the border of the imaging volume.

Movie S3. Two examples of wild-type cells (back to back) filmed in CEN IV-tracking assay transitioning from a syntelic to a bipolar attachment. Related to Figure 1
Image projections as in Movie S2. Note the jerky movements of the CEN IV tags during the period of splitting. This corroborates the notion of a tug of war between monopolar and bipolar attachment, perhaps with several rounds of detachment and reattachment in syntely before a bipolar attachment can separate the sisters, leading to stabilization.

Movie S4. Wild-type cell carrying the new symmetric CEN IV tag in CEN IV-tracking assay. Related to Figure 1
Image projections and data representation as in Movie S2. Marker 'Cen1' represents the position of both CEN IV tags.

Movie S5. Representative *ipl1-321* cell with unseparated tags in CEN IV-tracking assay. Related to Figure 2
Image projections and data representation as in Movie S2. Marker 'Cen1' represents the position of both CEN IV tags.

Movie S6. Three examples of *stu2-277* cells (back to back) in CEN IV-tracking assay. Related to Figure 3
Image projections and data representation as in Movie S2. The three cells are representative of the attachment states found in *stu2-277* cells. First cell has unseparated CEN tags, second cell has separated tags and third cell has detached tags. In the cases with unseparated tags marker 'Cen1' represents the position of both CEN IV tags. In the detached case note that while the state of attachment is difficult to make out by visual inspection, numerical analysis of the trajectories permits clear distinction between an attached and fully detached state (Jaqaman et al., 2007) (data not shown).

Movie S7. Two examples of *cin8Δ* cells (back to back) in CEN IV-tracking assay. Related to Figure 4

Image projections and data representation as in Movie S2. The first cell represents a case in which unseparated CEN tags cross the spindle midzone. Marker 'Cen1' represents the position of both CEN IV tags. The second cell represents a case displaying transiently separated CEN tags. Note that transient fusions of the two CEN IV tags result in an interpolated position for one of the two tags, indicated by an asterisk. In general, in these time points of transient fusions the image signal by the tags is exceedingly complex making automated (and visual) tracking difficult. However, the software locks in stably after clear separation of the CEN IV tags.

Table S1. Statistics from static CEN IV-snapshot assay. Related to Figures 1, 2, 3, and 4.

	WT 25°C Original tag	**WT 25°C Symmetric tag**	***ipl1-321* 37°C**	***stu2-277* 37°C**	***cin8Δ* 25°C**
Number of images	50	60	60	50	80
Number of cells	828	3817	1955	869	3339
Number of metaphase spindles	284	925	447	484	322
Number of detected unseparated tags	125	487	357	436	258
Number of detected separated tags	159	438	90	48	64
Final number of tags classified as unseparated	115	204	357	436	238
Final number of tags classified as separated	169	721	90	48	84
Percentage of unseparated tags	40.4	22.1	79.9	90.1	73.9
Percentage of separated tags	59.6	77.9	20.1	9.9	26.1

Table S2. Statistical analysis of SPB−CEN distances. Values are Mean ± SD. Related to Figures 1, 2, 3, and 4.

Mean distance: Uncertainty-weighted average of the SPB-CEN IV distances. *SD of distance*: Standard deviation of the SPB–CEN IV distances, weighted with the respective uncertainties. *AP-to-TP frequency*: Inverse of the average time the CEN IV-tag spent in antipoleward motion ('catastrophe frequency'). *TP-to-AP frequency*: Inverse of the average time the CEN IV-tag spent in poleward motion ('rescue frequency'). *Antipoleward speed*: Average speed by which the CEN IV-tag moved away from the pole calculated by piecewise linear fits to the SPB–CEN IV distance trajectories (see (Dorn et al., 2005) for details). *Poleward speed*: Average speed by which the CEN IV-tag moved toward from the pole calculated by piecewise linear fits to the SPB–CEN IV distance trajectories (see (Dorn et al., 2005) for details).

	WT 25°C all tags	**WT 37°C all tags**	***ipl1-321* 37°C all tags**	***stu2-277* 37°C all tags**	***cin8Δ* 25°C all tags**
Mean Distance (µm)	0.48 ± 0.08	0.56 ± 0.08	0.56 ± 0.09	0.51 ± 0.06	0.45 ± 0.11
AP-to-TP Frequency (1/s)	0.63 ± 0.01	0.64 ± 0.02	0.66 ± 0.02	0.68 ± 0.01	0.67 ± 0.01
TP-to-AP Frequency (1/s)	0.64 ± 0.01	0.64 ± 0.01	0.67 ± 0.02	0.69 ± 0.01	0.67 ± 0.01
Antipoleward Speed	2.79 ± 0.04	3.42 ± 0.08	4.15 ± 0.14	3.92 ± 0.08	3.77 ± 0.07
Poleward Speed (µm/min)	-2.83 ± 0.04	-3.50 ± 0.09	-4.16 ± 0.14	-3.94 ± 0.08	-3.69 ± 0.07
% of Midzone Crossings	10.64	19.15	6.45	9.09	60
Number of Cells	47	47	31	44	25

	WT 25°C unseparated tags	**WT 37°C unseparated tags**	***ipl1-321* 37°C unseparated tags**	***stu2-277* 37°C unseparated tags**	***cin8Δ* 25°C unseparated tags**
Mean Distance (µm)	0.47 ± 0.09	0.54 ± 0.07	0.53 ± 0.07	0.51 ± 0.06	0.45 ± 0.09
AP-to-TP Frequency (1/s)	0.63 ± 0.01	0.65 ± 0.02	0.69 ± 0.02	0.68 ± 0.01	0.67 ± 0.02
TP-to-AP Frequency (1/s)	0.62 ± 0.01	0.64 ± 0.02	0.68 ± 0.02	0.69 ± 0.01	0.67 ± 0.02
Antipoleward Speed	2.48 ± 0.05	3.14 ± 0.08	4.06 ± 0.17	3.80 ± 0.08	3.13 ± 0.09
Poleward Speed (µm/min)	-2.58 ± 0.05	-3.09 ± 0.08	-3.98 ± 0.16	-3.87 ± 0.08	-2.88 ± 0.09
% of Midzone Crossings	18.52	12.5	0	7.89	20
Number of Cells	27	40	23	38	10

	WT 25°C separated tags	**WT 37°C separated tags**	***ipl1-321* 37°C separated tags**	***stu2-277* 37°C separated tags**	***cin8Δ* 25°C separated tags**
Mean Distance (µm)	0.48 ± 0.08	0.67 ± 0.09	0.64 ± 0.13	0.59 ± 0.07	0.53 ± 0.12
AP-to-TP Frequency (1/s)	0.64 ± 0.01	0.63 ± 0.03	0.61 ± 0.04	0.67 ± 0.03	0.67 ± 0.01
TP-to-AP Frequency (1/s)	0.65 ± 0.01	0.64 ± 0.03	0.64 ± 0.04	0.67 ± 0.03	0.67 ± 0.02
Antipoleward Speed	3.04 ± 0.05	4.49 ± 0.27	4.34 ± 0.25	4.41 ± 0.19	4.06 ± 0.09
Poleward Speed (µm/min)	-3.04 ± 0.05	-5.13 ± 0.31	-4.56 ± 0.25	-4.21 ± 0.16	-4.09 ± 0.09
% of Midzone Crossings	0	57.14	25	16.67	86.67
Number of Cells	20	7	8	6	15

EXTENDED EXPERIMENTAL PROCEDURES

Yeast strains and growth conditions.
All yeast strains used in this study were haploid and derived from W303 (*MATa ade2-1 trp1-1 can1-100 leu2-3, 12 his3-11, 15 ura3 GAL psi*$^{+}$). The cells used in the kinetochore-snapshot assay had SPBs and kinetochores marked using SPC42-CFP and NDC80-GFP plasmids, respectively (He et al., 2001), integrated at their endogenous locus. The cells used in the CEN IV-tracking assay contained the −1.1 Ch IV TetO/TetR-GFP construct described in (He et al., 2000) and SPBs marked using a SPC42-GFP plasmid integrated at the endogenous locus (He et al., 2000). In the CEN IV-snapshot assay of wild-type and *cin8Δ* cells we integrated a TetR-3GFP plasmid and a construct with 11kb of TetO at +370bp from CEN IV. Cells in the tubulin assay had SPBs and tubulin tagged using SPC42-CFP and TUB1-GFP plasmids.

The new symmetric CEN IV tag was constructed as follows. Plasmids containing 6 kb of TetO tandem-repeats were inserted at −286 bp (AvrII site) and +390 bp (MfeI site) positions from the CEN IV start position. After integration, TetO repeats begin at −360bp and +370bp on each side of CEN IV. These two sets of TetO tandem-repeats thus are near perfectly symmetric around CEN IV. Most importantly, to our knowledge, they are significantly closer to the bona fide CEN IV sequence than any other CEN-proximal marker published to date. For each arm of Chromosome IV, the centroids of the TetO tandem repeats are approximately ~3.4 kb away from CEN IV. The level of compaction of the chromatin fiber in *S. Cerevisiae* interphase has been reported as 7–10 nucleosomes / 11 nm (110-150 bps / nm) based on optimized in situ hybridization and live imaging (Bystricky et al., 2004); or 1.2-2.4 nucleosomes / 11 nm (GC-rich) and 1.8-3.6 nucleosomes / 11 nm (AT-rich) based on chromosome conformation capture (3C) technology (Dekker, 2008). For the first estimation, assuming 125 bps / nm mass density, the one-arm tag is about 25 nm from the CEN IV position, and as a result the signals of the two one-arm tags are 50nm apart. The 3C data indicated a more extended chromatin fiber with compaction ratio about one fourth of the earlier estimation. This translates into 100 nm distance between the one-arm tags and the CEN IV position. Regardless of the difference between the estimations of compaction ratio, the signals emitted from the tags fall within the diffraction-limited volume of one point spread function.

Cells were prepared for microscopy as described in (Rines et al., 2004). In brief, cells were grown overnight at room temperature in SC-minimal media supplemented with 20 μg/ml of adenine and 2% glucose. *ipl1-321* and *stu2-277* cells were arrested in α-factor (5 μg/ml) for at least 2 h, and released at 37°C. A concentrated cell suspension (2.2 μl) was spotted onto an agarose-coated microscope slide and sealed with a coverslip before imaging. For the kinetochore-snapshot and tubulin assays, cells were treated cells with 2% formaldehyde for 5–10 min followed by 0.1 M phosphate buffer, pH 6.6, for at least 5 min and imaged at room temperature.

Microscopy
All images were acquired using a DeltaVision microscope with a 100x/1.4NA lens, mercury lamp illumination and a Photometrics CoolSnap HQ camera, except for images

in the CEN IV-snapshot assay using the symmetric tag design, which were obtained with a 100x/1.5NA TIRF lens and a solid state illumination lamp. The microscope was equipped with a heated chamber to maintain cells at controlled temperature during imaging. Voxel size for all experiments was 0.066x0.066x0.20 µm. 4D image sizes {x,y,z,t} for the different assays were as follows: {160,160,24,1} for the kinetochore-snapshot assay, {64,64,16,100–300} for the CEN IV-tracking assay (sampling rate of 1 Hz), and {1024,1024,30,1} for the CEN IV-snapshot assay. Exposure times for a single slice were as follows: 700 ms for the kinetochore-snapshot assay, 47 ms for the CEN IV-tracking assay and 250ms for the CEN IV-snapshot assay. At the beginning and end of each movie, five additional frames were acquired with closed camera shutter for dark frame subtraction as a way to correct for charge-coupled device chip dependent effects.

CEN IV-tag tracking with super-resolution

Image analysis for the CEN IV-tracking and -snapshot assays was performed as described previously (Dorn et al., 2005), using a two-step algorithm for detecting spots in single frames, followed, in time-lapse image data, by tracking and refinement of the spot detection.

The two steps of spot detection in single frames are (1) identification of candidate positions, and (2) super-resolution fitting of spot signals. Candidate spot positions were identified as local maxima of 3D frames filtered by a 3D Gaussian filter matched to the point-spread-function (PSF) of the microscope. To distinguish between local maxima originating from signal and noise, respectively, we used unimodal thresholding of the estimated signal-to-noise ratio of the maxima (Jaqaman et al., 2010). To estimate the positions of isolated signals with sub-pixel accuracy, and to distinguish signals separated by less than the resolution limit, we fitted candidate local maxima with 3D Gaussians whose size had been matched to the empirical PSF of the microscope, which was ~1.3 times wider than the theoretical PSF. To account for tags that were separated by less than the resolution limit of the microscope, and thus only resulted in one local maximum, we fitted each local maximum with an additional Gaussian. If two Gaussians fit the intensity distribution around the local maximum significantly better than a single Gaussian (F-test, 5% threshold), we considered that a spot consisted of two fluorescent tag. Otherwise, we retained the single-Gaussian fit. Thus, we were able to identify spindle pole body and centromere tag signals that were separated by less than 65% of the resolution limit of the microscope (Dorn et al., 2005).

In time-lapse movies, fluorescent tags were tracked through time by first assigning nearest-neighbor links between all the frames that contained the maximum number of detected tags (source frames). Then, links were propagated to frames with fewer detected tags (target frames) to ensure correct identification of the tags. The position of missing tags in target frames was estimated using linear interpolation between source frames. The position measurements and estimates were used to resolve missing tags and to improve the estimated position of detected tags by a template-matching algorithm. Fluorescence intensity distributions from source frames were used as templates that were fitted to the measured and estimated tag positions. If possible, every source frame was fitted from four other source frames, while every target frame was fitted using distributions from the five closest source frames. These fits returned the relative displacement of tags between

frames. The final positions and uncertainties were obtained by solving a system of linear equations comprising both the absolute position measurements from the spot detection and the relative position measures from the template matching steps. Thus, we were able to both recover fluorescent tags that had been missed during the single-frame detection step, and to improve the position estimation of already detected signals.

Fitting of both spot signals and intensity templates also returned positional uncertainties, which we subsequently used for statistical data analysis.

Tag Assignment

Since the intensity of the unseparated centromere tags was similar to the intensity of the SPB tags, we used spindle geometry to assign tag labels. Budding yeast undergoes closed mitosis with SPBs embedded in the nuclear membrane (Jaspersen and Winey, 2004). Therefore, SPBs exhibit less movement than CEN tags, which is particularly obvious when tracking tags in 3D (McAinsh et al., 2003; Thomann et al., 2002). Moreover, because SPBs are forcibly located at the nuclear periphery, they are normally the two most distant tags. This is further supported by electron microscopy data showing that kinetochore microtubules are relatively well-aligned with the pole-to-pole axis (O'Toole et al., 1999) and thus CEN positions tend to lie in between SPBs. Consequently, the tag pair with the largest and most stable inter-tag distance was selected as the SPBs. When the centromere tags were resolvable, we assigned each one to the closer of the two SPBs (Thomann et al., 2003). When the tags were unresolvable and only one spot was detected, we assigned that spot to the closer SPB and assumed it represented two kinetochores.

Computational correction of chromatic aberration

To correct for chromatic aberrations between the channels in two-color images, we employed a two-step algorithm: To correct for gross aberrations, we performed an initial alignment based on chromatic aberration measured from images of spindle pole bodies labeled with both CFP and YFP. However, more subtle chromatic aberration depends on the position of the fluorescent probes relative to the objective of the microscope (Joglekar et al., 2009). Thus, we performed a second computational alignment step, which was based on the assumption that there is less Ndc80p (or Tub1p) at the spindle pole bodies than there is between the spindle pole bodies, and that the intensity is distributed along the spindle axis. These assumptions hold for all but monopolar distributions of kinetochores. The alignment algorithm shifted the voxel grid used to read-out kinetochore or tubulin intensities along the pole-to-pole axis until the fluorescence intensity at both poles was jointly minimized. This resulted in visually excellent alignment of channels, and allowed us to appropriately combine the spatial distribution of fluorescence intensities from different images.

Normalization of signal in V-plots

In V-plots, the intensity distribution for a given spindle length is plotted along a horizontal strip, with color reflecting the intensity. Longer spindles are visualized as longer strips, resulting in a V-shaped appearance of the plot. To give a smooth appearance to the plot, the intensity distribution from each experiment was blurred along the vertical axis using a triangle filter of 0.1 μm width. Since the number of Ndc80p molecules can be considered constant throughout mitosis (Joglekar et al., 2009), we

normalized the total Ndc80-GFP signal for each spindle length to 1. In contrast the amount of tubulin in the spindle is spatially and temporally variable, so that normalization was impossible. Data in the tubulin assay is rescaled so that the maximum intensity is always 1. To ensure comparable data, we performed all experiments on the same microscope with the same settings.

Analysis of directional instability of chromosomes measured in the CEN IV-tracking assay

Data in Table S2 were obtained from the tag positions as described previously (Dorn et al., 2005). SPB–CEN IV distances and there uncertainty was calculated as the 3D distance between corresponding tags and their positional uncertainties, respectively.

Reclassification of unseparated tags in CEN IV-snapshot assay

Analysis of live cell CEN-tag dynamics revealed, that several imaging artifacts could result in temporarily undetected CEN IV tags on bioriented chromosomes. Presence of 4 tags in at least 1 time point of a CEN IV-tracking movie allowed us to classify the sister kinetochores as bioriented from this time point onward. Undetected tags could arise from the presence of stretching or due to close proximity between a CEN IV tag to the SPB (notice that our software detects these distances with super-resolution to below 200 nm; thus, undetected tags due to CEN IV–SPB proximity were the rarer of the two scenarios). The same imaging artifacts could also affect the CEN IV-snapshot, requiring a method to reclassify apparently 3-tagged cells as possibly bioriented.

Here, we made use of the information from CEN IV-tracking assay, in which bipolarity can be detected with high confidence. First we determined the distributions $P(i \mid s)$ defining the probability of observing a given intensity i for a tag in a state (s = bipolar and s = syntelic); and $P(s \mid l)$ defining the probability of observing state s for a given spindle length l (Figs S2B and S2D; and Figs S3C and S3E).

Given the observation of an unseparated tag of intensity i in spindle of length l in the CEN IV-snapshot assay, the posterior probability $P(s \mid i, l)$ for the kinetochore sisters to be in either one of the two states s = bipolar or s = syntelic, is given by:

$$P(s|i,l) = \frac{P(i \mid s,l)P(s \mid l)}{P(i \mid l)} = \frac{P(i \mid s)P(s \mid l)}{\sum_{s'} P(i \mid s')P(s' \mid l)}$$

Each cell with unseparated tags was assigned to the class with maximum posterior probability.

To obtain uncertainties in our estimates we repeated the full reclassification procedure with cells obtained from 1000 bootstrap samples with replacement. White solid and dashed lines (in Figures 1J, 1L and similar ones) represent Mean ± SD estimates.

Conversion between spindle lengths and time

To convert the observed experimental data for bipolarity progression at different spindle lengths (Figure 1L) into a temporal progression curve (Figure S3I) we used the following procedure: We set the time it takes for the spindle to grow from 1.2 to 2 microns in length as 30 minutes and assumed that the slope of the cumulative histogram of Figure 1J for

WT indicates the inverse of the progression speed. The temporal progression of bipolarity establishment in *ipl1-321*cells was computed analogously. However, these cells entered anaphase typically only at a spindle length of 3 μm. Assuming that the spindle elongation rates are roughly equal to those in WT cells the time span used for the conversion was 60 minutes instead of 30 minutes.

Prediction of FRAP on kinetochore proteins from single chromosome analysis of biorientation

Previous work from (Pearson et al., 2004) measured fluorescence recovery after photobleaching (FRAP) of the centromere histone-H3 CENP-A/Cse4p-GFP. After DNA replication Cse4p is a physically stable centromere component. Therefore, recovery of fluorescence after photobleaching one of the two bilobes would indicate, 1) one-sided detachment of a bioriented kinetochore pair followed by recoil of the pericentric DNA of the loose kinetochore into the bleached bilobe containing the still attached kinetochore; 2) oscillations between the two lobes of bioriented, yet tension-free sisters ('amphitelic oscillations'); or 3) resolution of syntely, in which one of the two sister kinetochores changes side from one half-spindle to the other. On individual recovery curves the authors observed recoveries up to 19%. On average, 10 minutes after photobleaching the reported recovery was 4.5 ± 7.3 % (mean ± SD; $n = 9$) and a smaller value of 2.2 ± 4.4 % (mean ± SD; $n = 9$) at 20 minutes after photobleaching. Based on these data the authors concluded that the frequency of one-sided detachments or amphitelic oscillations was low. However, Pearson and colleagues did not explicitly discuss the possibility of FRAP due to syntely resolution, because the premise of their interpretation was that bilobes are synonymous for biorientation. According to the model we propose here, the reported FRAP values could also be associated with a scenario in which one of the sisters of a newly bioriented kinetochore pair is pulled across the spindle equator. If the percentage of syntely at a given time in mitosis is *S* the percentage of fluorescence recovery due to syntely resolution will be *S/2*. Using the data in Figure 1L, we first converted the curve of gradual biorientation into a time progression curve (see previous section and Figure S3I). We then chose in this curve 1000s as the time point of virtual photobleaching. This time point corresponds to a spindle length of ~1.5 μm, which was used for the FRAP experiments by (Pearson et al., 2004). After 1000s, the change in number of syntelic attachments in Figure S3I was converted into a predicted FRAP value as a function of time (Figure S3J), with an asymptotic recovery of ~12%. From this we conclude that the FRAP measurements published by (Pearson et al., 2004) would be completely consistent also with our model of gradual biorientation.

Supplemental References

Bystricky, K., Heun, P., Gehlen, L., Langowski, J., and Gasser, S.M. (2004). Long-range compaction and flexibility of interphase chromatin in budding yeast analyzed by high-resolution imaging techniques. Proceedings of the National Academy of Sciences of the United States of America *101*, 16495-16500.

Dekker, J. (2008). Mapping in vivo chromatin interactions in yeast suggests an extended chromatin fiber with regional variation in compaction. The Journal of biological chemistry *283*, 34532-34540.

Dorn, J.F., Jaqaman, K., Rines, D.R., Jelson, G.S., Sorger, P.K., and Danuser, G. (2005). Yeast kinetochore microtubule dynamics analyzed by high-resolution three-dimensional microscopy. Biophys J *89*, 2835-2854.

He, X., Asthana, S., and Sorger, P.K. (2000). Transient sister chromatid separation and elastic deformation of chromosomes during mitosis in budding yeast. Cell *101*, 763-775.

He, X., Rines, D.R., Espelin, C.W., and Sorger, P.K. (2001). Molecular analysis of kinetochore-microtubule attachment in budding yeast. Cell *106*, 195-206.

Jaqaman, K., Dorn, J.F., Marco, E., Sorger, P.K., and Danuser, G. (2007). Phenotypic clustering of yeast mutants based on kinetochore microtubule dynamics. Bioinformatics *23*, 1666-1673.

Jaqaman, K., King, E.M., Amaro, A.C., Winter, J.R., Dorn, J.F., Elliott, H.L., McHedlishvili, N., McClelland, S.E., Porter, I.M., Posch, M., *et al.* (2010). Kinetochore alignment within the metaphase plate is regulated by centromere stiffness and microtubule depolymerases. J Cell Biol *188*, 665-679.

Jaspersen, S.L., and Winey, M. (2004). The budding yeast spindle pole body: structure, duplication, and function. Annual review of cell and developmental biology *20*, 1-28.

Joglekar, A.P., Bloom, K., and Salmon, E.D. (2009). In vivo protein architecture of the eukaryotic kinetochore with nanometer scale accuracy. Current biology : CB *19*, 694-699.

McAinsh, A.D., Tytell, J.D., and Sorger, P.K. (2003). Structure, function, and regulation of budding yeast kinetochores. Annual review of cell and developmental biology *19*, 519-539.

O'Toole, E.T., Winey, M., and McIntosh, J.R. (1999). High-voltage electron tomography of spindle pole bodies and early mitotic spindles in the yeast Saccharomyces cerevisiae. Mol Biol Cell *10*, 2017-2031.

Pearson, C.G., Yeh, E., Gardner, M., Odde, D., Salmon, E.D., and Bloom, K. (2004). Stable kinetochore-microtubule attachment constrains centromere positioning in metaphase. Current biology : CB *14*, 1962-1967.

Rines, D., Thomann, D., Dorn, J., Goodwin, P., and Sorger, P.K. (2004). Live cell imaging of yeast. In Live Cell Imaging: A Laboratory Manual R.D. Goldman, and D.L. Spector, eds. (Cold Spring Harbor Laboratory Press, Woodbury, NY.), p. 631.

Thomann, D., Dorn, J., Sorger, P.K., and Danuser, G. (2003). Automatic fluorescent tag localization II: Improvement in super-resolution by relative tracking. J Microsc *211*, 230-248.

Thomann, D., Rines, D.R., Sorger, P.K., and Danuser, G. (2002). Automatic fluorescent tag detection in 3D with super-resolution: application to the analysis of chromosome movement. J Microsc *208*, 49-64.

Figure S1

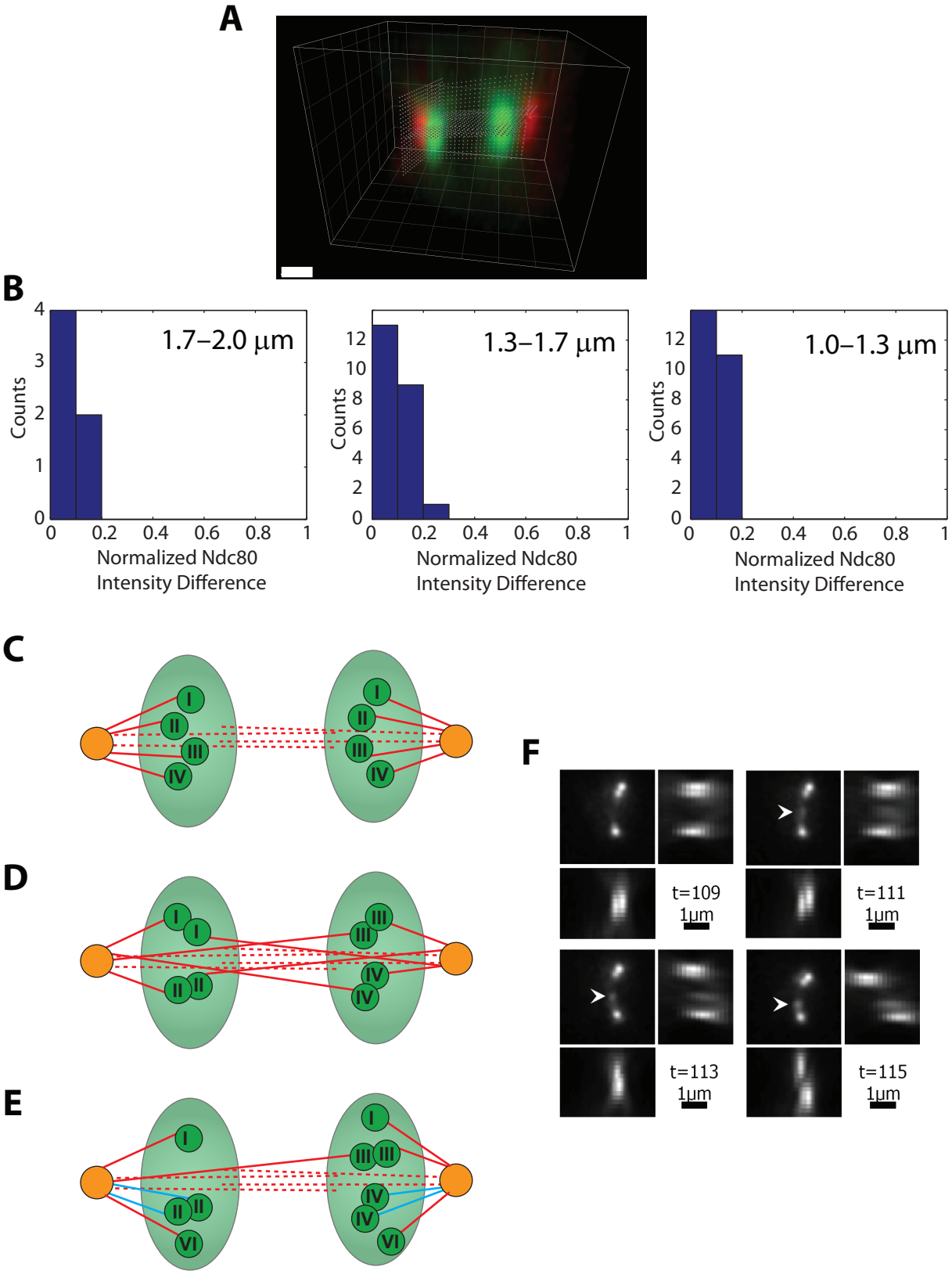
A
B
1.7–2.0 μm
1.3–1.7 μm
1.0–1.3 μm
Counts
Normalized Ndc80
Intensity Difference
C
D
E
F
t=109
1μm
t=111
1μm
t=113
1μm
t=115
1μm

Figure S2

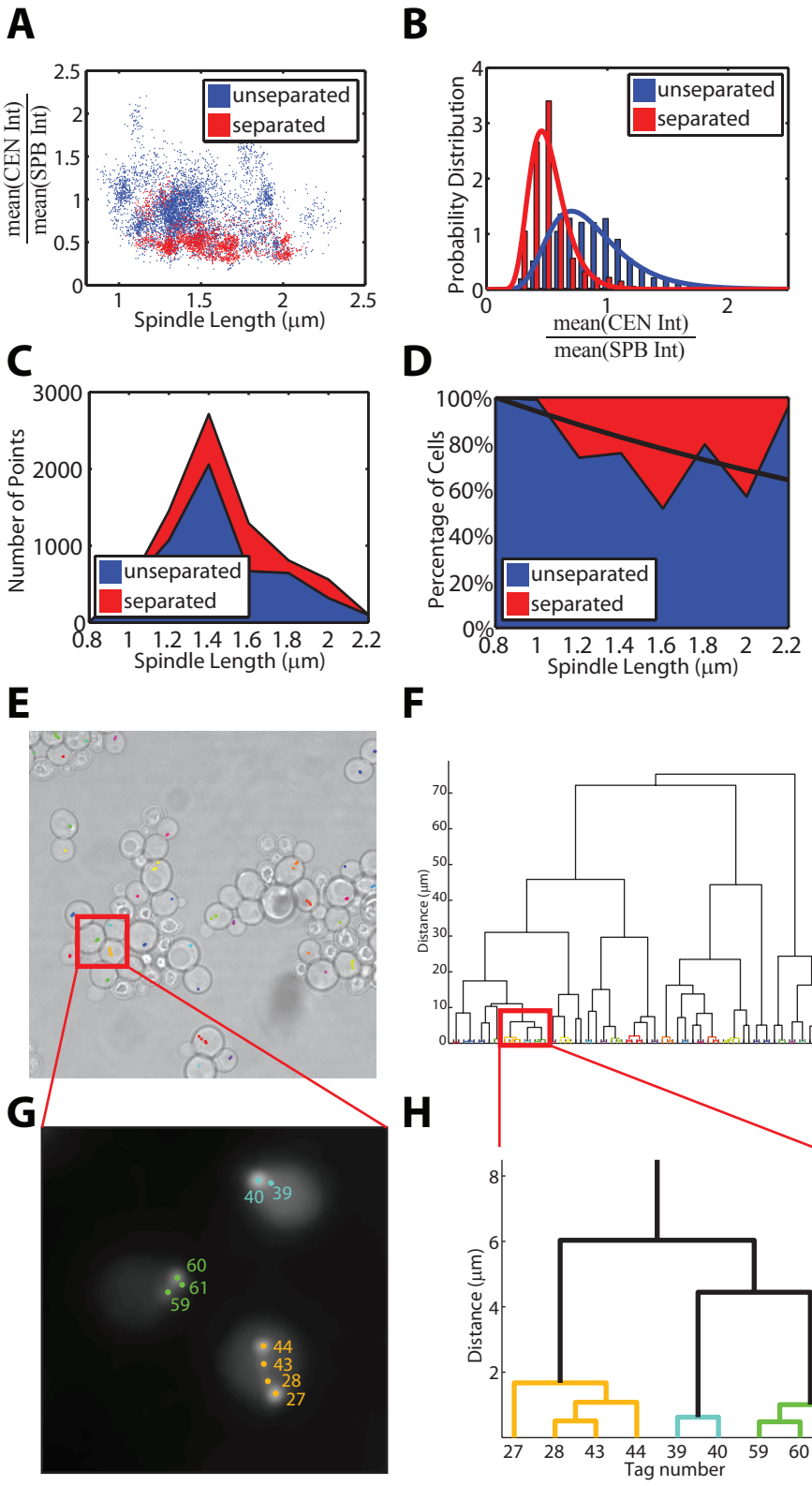
A
mean(CEN Int) / mean(SPB Int)
Spindle Length (μm)
unseparated
separated
B
Probability Distribution
mean(CEN Int) / mean(SPB Int)
unseparated
separated
C
Number of Points
Spindle Length (μm)
unseparated
separated
D
Percentage of Cells
Spindle Length (μm)
unseparated
separated
E
F
Distance (μm)
G
40 39
60
61
59
44
43
28
27
H
Distance (μm)
27 28 43 44 39 40 59 60 61
Tag number

Figure S3

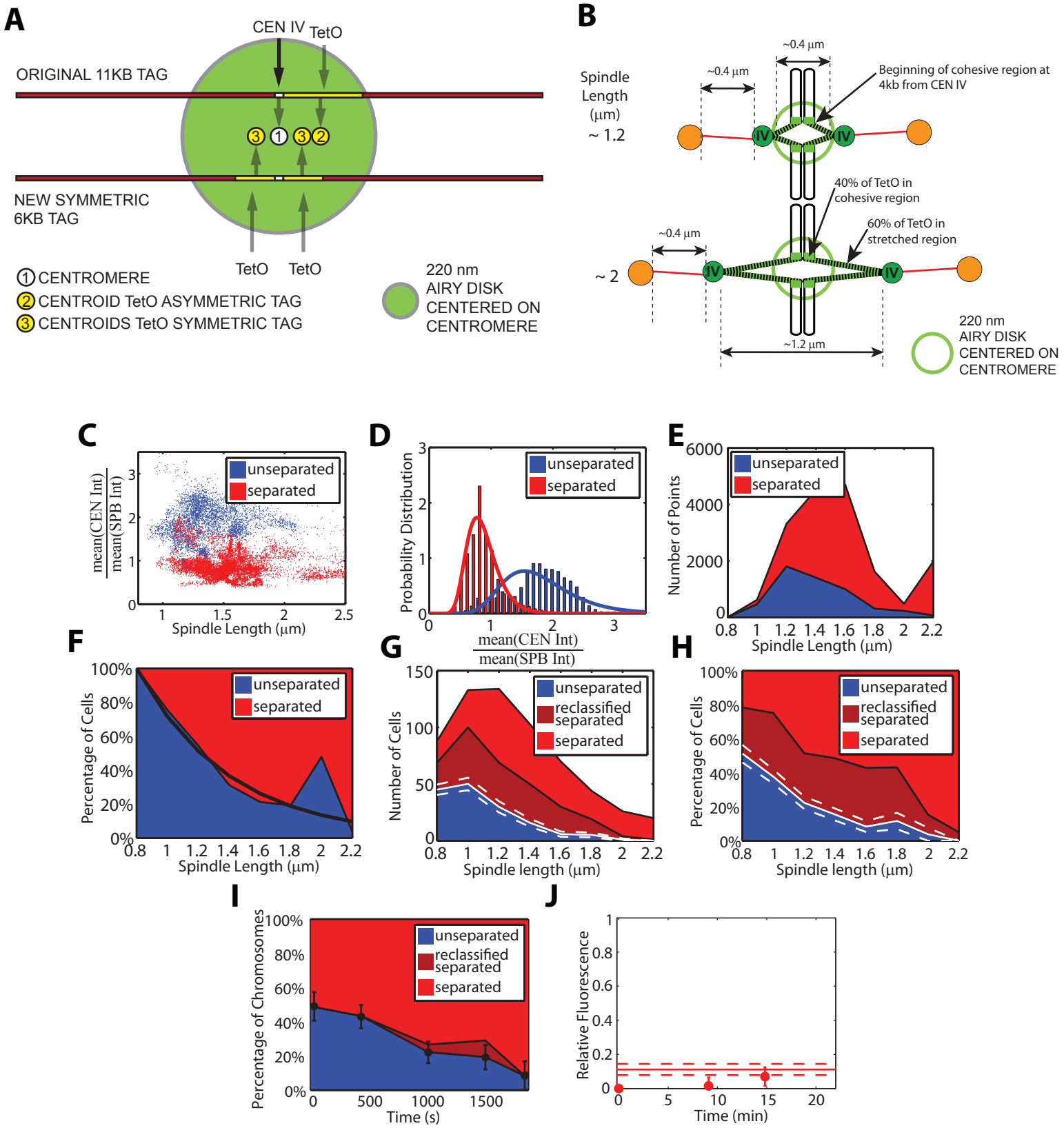
A
CEN IV
TetO
ORIGINAL 11KB TAG
NEW SYMMETRIC 6KB TAG
TetO
TetO
1 CENTROMERE
2 CENTROID TetO ASYMMETRIC TAG
3 CENTROIDS TetO SYMMETRIC TAG
220 nm AIRY DISK CENTERED ON CENTROMERE
B
Spindle Length (µm)
~ 1.2
~ 2
~0.4 µm
Beginning of cohesive region at 4kb from CEN IV
40% of TetO in cohesive region
60% of TetO in stretched region
~1.2 µm
220 nm AIRY DISK CENTERED ON CENTROMERE
C
mean(CEN Int) / mean(SPB Int)
Spindle Length (µm)
unseparated
separated
D
Probability Distribution
E
Number of Points
F
Percentage of Cells
G
Number of Cells
reclassified separated
H
I
Percentage of Chromosomes
Time (s)
J
Relative Fluorescence
Time (min)

Figure S4

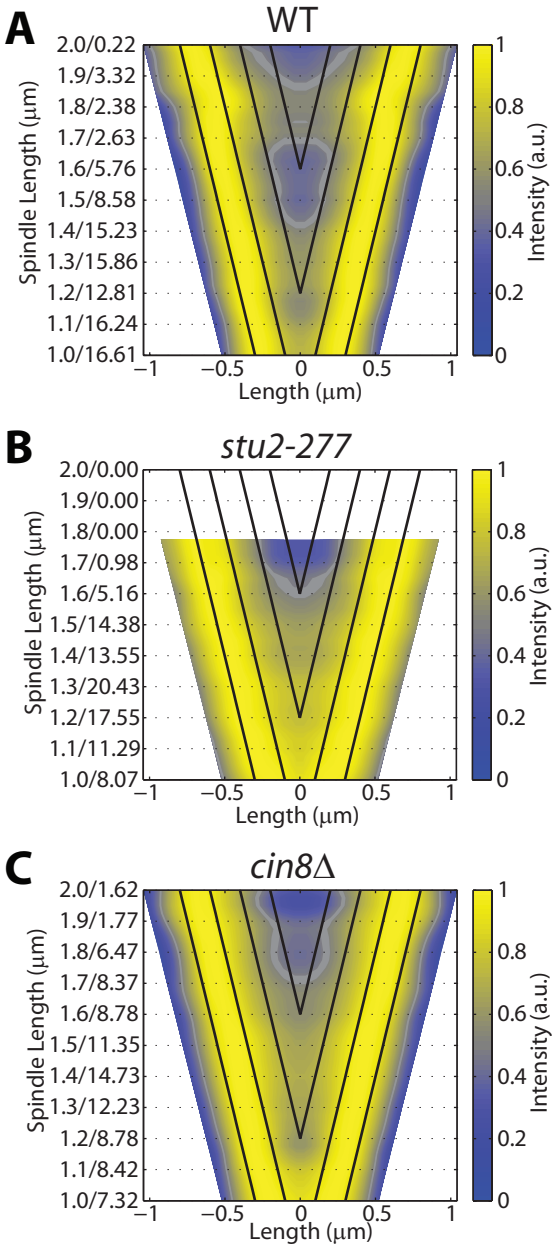
A
WT
2.0/0.22
1.9/3.32
1.8/2.38
1.7/2.63
1.6/5.76
1.5/8.58
1.4/15.23
1.3/15.86
1.2/12.81
1.1/16.24
1.0/16.61
Spindle Length (μm)
−1
−0.5
0
0.5
1
Length (μm)
1
0.8
0.6
0.4
0.2
0
Intensity (a.u.)
B
stu2-277
2.0/0.00
1.9/0.00
1.8/0.00
1.7/0.98
1.6/5.16
1.5/14.38
1.4/13.55
1.3/20.43
1.2/17.55
1.1/11.29
1.0/8.07
Spindle Length (μm)
−1
−0.5
0
0.5
1
Length (μm)
1
0.8
0.6
0.4
0.2
0
Intensity (a.u.)
C
cin8Δ
2.0/1.62
1.9/1.77
1.8/6.47
1.7/8.37
1.6/8.78
1.5/11.35
1.4/14.73
1.3/12.23
1.2/8.78
1.1/8.42
1.0/7.32
Spindle Length (μm)
−1
−0.5
0
0.5
1
Length (μm)
1
0.8
0.6
0.4
0.2
0
Intensity (a.u.)

Figure S5

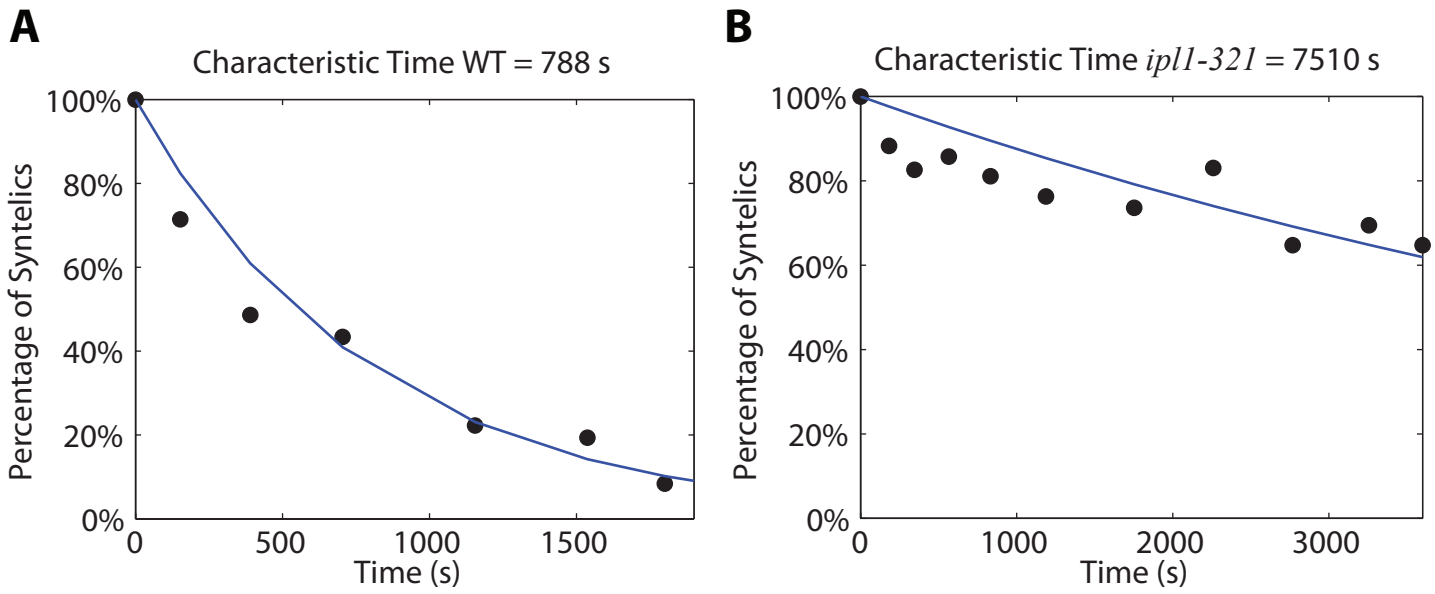
A
Characteristic Time WT = 788 s
Percentage of Syntelics
100%
80%
60%
40%
20%
0%
0
500
1000
1500
Time (s)
B
Characteristic Time ipl1-321 = 7510 s
Percentage of Syntelics
100%
80%
60%
40%
20%
0%
0
1000
2000
3000
Time (s)